

Pressure, volume, density relationships in the plasma sheet

Richard L. Kaufmann

Department of Physics, University of New Hampshire, Durham, New Hampshire, USA

W. R. Paterson and L. A. Frank

Department of Physics and Astronomy, University of Iowa, Iowa City, Iowa, USA

Received 11 November 2003; revised 11 March 2004; accepted 18 June 2004; published 13 August 2004.

[1] Long-term-averaged three-dimensional data-based models of the plasma sheet were used to study relationships between the density n , pressure P , and temperature T of the plasma and between the volume V and particle content N of a tube that contains 1 Wb of magnetic flux. Near midnight a typical unit flux tube located at $x_0 = -11.5 R_E$ was found to contain only 30% as many particles as a typical unit flux tube located at $x_0 = -29.5 R_E$. The average value of the adiabatic compression parameter $PV^{\delta/3}$ was only 20% and 15% as large at $x_0 = -11.5 R_E$ for ions and electrons, respectively, as at $x_0 = -29.5 R_E$. A decrease of the average N and $PV^{\delta/3}$ can be caused by the ejection of plasmoids during reconnection. Such ejections are likely to be important beyond $20 R_E$. Fast flows, flux tube interchange, drift effects, and a heat flux are likely to be more important at lower altitudes. The entropy parameter $Pn^{-5/3}$ was found to be relatively uniform throughout the region studied. The energy parameter $TV^{2/3}$ decreased by 40% for ions and 10% for electrons near midnight between -29.5 and $-11.5 R_E$. These energy parameter changes suggest that the most energetic ions and electrons are either being deenergized or preferentially lost, processes that may be associated with gradient and curvature drifts through the sides of the convecting flux tubes or by wave instabilities and a parallel heat flux.

INDEX TERMS: 2764 Magnetospheric Physics: Plasma sheet; 2744 Magnetospheric Physics: Magnetotail; 2760 Magnetospheric Physics: Plasma convection; 2740 Magnetospheric Physics: Magnetospheric configuration and dynamics; **KEYWORDS:** plasma sheet, magnetotail, pressure balance inconsistency, 3-D models

Citation: Kaufmann, R. L., W. R. Paterson, and L. A. Frank (2004), Pressure, volume, density relationships in the plasma sheet, *J. Geophys. Res.*, 109, A08204, doi:10.1029/2003JA010317.

1. Introduction

1.1. Modeling Techniques

[2] The present paper uses long-term-averaged three-dimensional (3-D) data-based models to extend earlier thermodynamic studies of the plasma sheet. The models are based on 8 years of Geotail measurements taken while the satellite perigee and apogee were 10 and $30 R_E$. Magnetic field measurements were made by the magnetic field (MGF) detector [Kokubun *et al.*, 1994] and particles were measured by the Comprehensive Plasma Instrument (CPI) detectors [Frank *et al.*, 1994]. Approximately 100,000 one-minute averages were made per year within the plasma sheet. The fluid variables were evaluated on the ground by integrating over the electron and ion distribution functions after corrections for satellite potential, background, and detector calibrations were made.

[3] The techniques used to create the plasma sheet models were described by Kaufmann *et al.* [2002, 2003]. Briefly, particle and field observations were sorted into 3×3 or $6 \times 6 R_E$ (x, y) boxes, where x and y are in

GSM coordinates. Data within each (x, y) box also were binned into eight β_x ranges, where β_x is the usual plasma β parameter with $B_x^2/2\mu_0$ used for the magnetic field pressure rather than $B^2/2\mu_0$. The average particle density, velocity, and pressure and the average magnetic field in each (x, y, β_x) box were combined with the constraint of long-term-averaged x -force balance and then used to calculate the z thickness of each box. All z locations in this paper refer to these calculated distances from the neutral sheet. The model particle densities also were consistent with force balance in the z direction and agreed with the available measurements of the electron plasma frequency, as described by Kaufmann *et al.* [2001]. Since ion count rates were low, there was no detectable degradation of the ion sensitivity over the 8 year period. Electron detector count rates were much higher, so electron geometry factors were adjusted annually to maintain charge neutrality in the models.

[4] As noted above, two of the principal advantages of the data-based models used here are that they are 3-D and force balanced in both the x and z directions. The divergence of the full pressure tensor and the inertial term were included in the momentum equation to satisfy the x force balance constraint. In contrast, Zaharia and Cheng [2003]

showed that it is hard to attain x force balance when adding a distribution of plasma to some empirical magnetosphere models. The 3-D nature of the models permits us to study both variations with respect to x and y within the neutral sheet and also variations of all parameters as one moves along an average flux tube.

[5] One substantial limitation of our models is that long-term averages are needed when using data from a single satellite to model the entire central plasma sheet (CPS). The minute-to-minute fluctuations of some parameters are larger than their long-term averages in the CPS [Angelopoulos *et al.*, 1993; Borovsky *et al.*, 1997]. Another important advantage and an associated limitation arose from the use of the same averaging methods to evaluate the magnetic field and all plasma parameters. This consistent treatment of plasma and field parameters produced magnetic field, ion, and electron models that are well matched within the plasma sheet. However, the calculation of z box thicknesses plus the use of averaged magnetic field components completely determines the shapes of magnetic field lines. We therefore cannot also add the constraint that $\nabla \cdot \mathbf{B} = 0$, which is usually included when creating empirical magnetic field models [Israelevich *et al.*, 2001]. The ratio $\nabla \cdot \mathbf{B} / \nabla \times \mathbf{B}$ was evaluated throughout the modeling region to check the unphysical deviations from $\nabla \cdot \mathbf{B} = 0$. This ratio was approximately 0.1 throughout the region studied here.

1.2. Plasma Parameters and Organization

[6] The present paper is an extension of our recent work which investigated the double adiabatic invariants, scattering, the average magnetization, and currents in the plasma sheet. This recent work showed that scattering and the effects of chaotic orbits were strong enough so that the adiabatic invariants of individual ions and electrons were not well conserved. Magnetization and guiding center drift currents were found to partially cancel, so each was stronger than the total cross-tail current near the neutral sheet.

[7] Erickson and Wolf [1980] pointed out a problem they encountered when comparing satellite data to the adiabatic equation of state

$$S_\sigma^V \equiv P_\sigma V^{5/3} = \text{constant} \quad (1)$$

along average drift paths. In the above, $P_\sigma = 1/3 \text{Tr}(\mathbf{P}_\sigma)$ is the isotropic part of the ion or electron pressure tensor, where σ is i or e for ions or electrons, and

$$V(x_0, y_0) = \int (1/B) ds \quad (2)$$

is the volume of a tube containing 1 Wb of magnetic flux and reaching the neutral sheet at (x_0, y_0) .

[8] The problem encountered by Erickson and Wolf [1980] was that realistic long-term-averaged models of plasmas and fields in the magnetotail did not satisfy equation (1). Schindler and Birn [1982] reached the same conclusion. It was suggested that convection was inherently unsteady.

[9] Hau *et al.* [1989], Erickson [1992], and Lemon *et al.* [2003] created force-balanced plasma and magnetic field models which satisfy equation (1). These force-balanced models required a deep minimum of B_z in the inner

magnetotail and differed substantially from the existing data-based magnetic field models.

[10] Sections 2 through 4 show models of the basic plasma parameters examined in this paper. The remaining sections provide brief analyses of some of these experimental results. Section 2 confirms the conclusions of previous studies [Erickson and Wolf, 1980; Schindler and Birn, 1982; Kivelson and Spence, 1988; Pontius and Wolf, 1990; Borovsky *et al.*, 1998; Chen and Wolf, 1999; Garner *et al.*, 2003] that equation (1) is not satisfied in long-term-averaged models of the CPS. Neither the flux tube content N nor S_σ^V is constant along an average drift path. An observer moving earthward would see large reductions of both N and S_σ^V .

[11] The relationship of the average particle energy or temperature to V was discussed by Wolf [1983] and Heinemann and Wolf [2001], who showed that an energy invariant

$$\lambda_\sigma = T_\sigma V^{2/3} \quad (3)$$

exists if plasma particles remain isotropic through elastic pitch angle scattering. In equation (3), T_σ is the temperature in energy units, $P_\sigma = n_\sigma T_\sigma$. Observations of λ_σ are presented in section 3.

[12] A number of studies examined relationships between P_σ and n_σ rather than between P_σ and V because both P_σ and n_σ are directly measured on most satellites, while V is not. These studies used a polytropic equation in the form

$$S_\sigma^n = P_\sigma n^{-\gamma} = \text{constant}. \quad (4)$$

The entropy of an average particle in an ideal monatomic gas is $s_\sigma = (3/2) \ln(S_\sigma^n)$, with $\gamma = 5/3$. Equation (4) with $\gamma = 5/3$ would be the same as equation (1) if the number of particles in a moving flux tube was conserved. The observed pressure-density relationships are shown in section 4.

[13] Tsyganenko [1982] and Kivelson and Spence [1988] suggested that cross-tail drift can result in the depletion of flux tube content as the tubes drift earthward. Erickson and Wolf [1980] and Borovsky *et al.* [1998] suggested that earthward particle decreases could be attributed to reconnection and the particle loss in plasmoids. Pontius and Wolf [1990] proposed a mechanism involving flux tube interchange that also could explain the decrease in the content of an average flux tube as one moves earthward. These mechanisms are discussed in sections 5 and 6.

2. Observed Pressure-Volume Relationships

2.1. Flux Tube Volume, Content, and Uncertainties

[14] Model field lines derived using 6 years of Geotail data were shown in Figure 1 of Kaufmann *et al.* [2003]. The field lines based on 8 years of data are similar. The integral in equation (2) was carried out along these field lines to determine the volume of a unit flux tube from the neutral sheet, $z = 0$, out to $|z| = 5 R_E$ for those lines which could be traced this far in our models. The set of 70 field lines used for this study began at $3 R_E$ increments from $x_0 = -29.5$ to -11.5 and $y_0 = -13.5$ to $13.5 R_E$. About half of these field lines reached $|z| = 5 R_E$ within the region that could be studied using Geotail data, and the other half could be traced to at

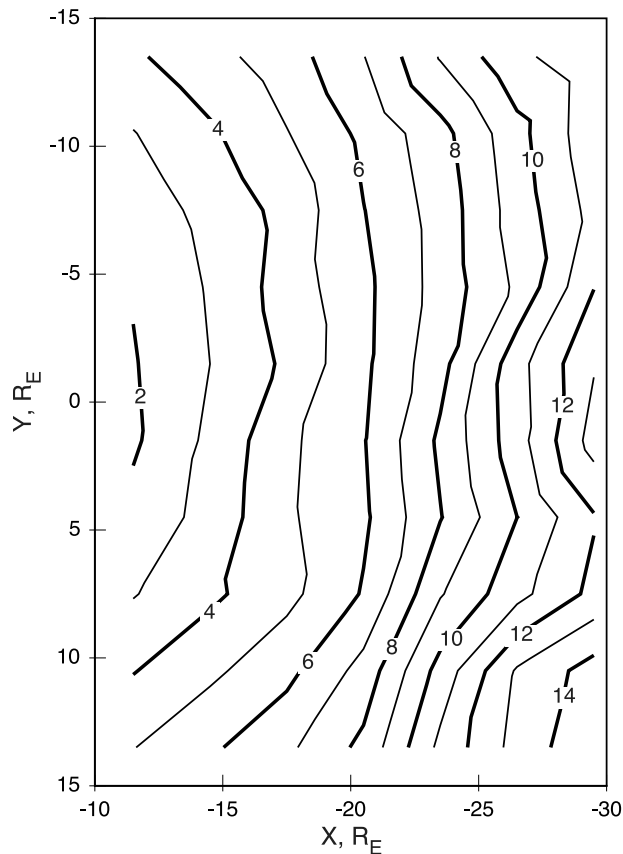


Figure 1. Volume per hemisphere, V in 10^{15} m^3 , of tubes containing 1 Wb of magnetic flux.

least $|z| = 3 R_E$. The Kp = 2 version of the T89 [Tsyganenko, 1989] magnetic field model was used in equation (2) to evaluate the volumes of those portions of the flux tubes starting at the largest $|z|$ that could be studied using our models and extending down to the ionosphere. Since the cross-sectional area of a unit flux tube is $1/B$ and since B is much smaller at $z = 0$ than at $|z| = 3$ to $5 R_E$, almost all the flux tube volume came from the portion of the integral that was evaluated using our models. The contribution to V from the region integrated using T89 was $<5\%$ for about half the field lines and $<10\%$ for all others except a few closest to the flanks. Since the empirical model was used only in regions with very little flux tube volume, the specific characteristics of T89 or of any alternative empirical model would have little effect on the results presented here.

[15] Figure 1 is a plot of the volumes, in one hemisphere, of tubes containing 1 Wb of magnetic flux. For comparison, a similar plot using T89 everywhere produced flux tube volumes about 10% smaller than those in Figure 1 between $x = -10$ and $x = -20 R_E$. The T89 flux tube volumes increased more slowly than ours beyond $x = -20 R_E$ so the difference in volumes increased to 30% at $x = -30 R_E$. The jagged appearance of Figure 1 is caused by the use of $3 \times 3 R_E$ (x, y) boxes for the initial binning. Plots created using these smaller boxes are shown when the principal features can be seen clearly. Some parameters have such large box-to-box fluctuations that multiple small peaks and valleys in the plots obscure the structure. In such cases the smoother plots created from $6 \times 6 R_E$ binning will be shown. The smoothing

produced by use of the larger boxes can, however, significantly reduce the calculated gradients of plasma parameters.

[16] Statistical errors are hard to evaluate. Standard deviations of the 1-min-averaged data points were calculated. Many of these standard deviations were comparable to the long-term-averaged values of the parameters being measured. The statistical error is the standard deviation divided by the square root of the number of independent measurements. We kept track of the number of 1-min-averaged data points in each (x, y, β_x) box and of the number of orbits contributing data points to each (x, y) box. For most parameters the point to point fluctuations during any one orbit were substantially smaller than the orbit to orbit fluctuations. With $6 \times 6 R_E$ binning, each orbit that entered a given (x, y, β_x) box contributed up to 100 one-minute data points to the box average. This large difference between the total number of data points and the number of different orbits contributing to a box average makes it hard to estimate the number of truly independent measurements. The error estimates in this paper are based partially on examining the standard errors calculated using both the number of points and the number of orbits. Examining box-to-box fluctuations and results from different sets of calculations often provided better error estimates. Runs using 3×3 and $6 \times 6 R_E$ boxes were compared. The $6 \times 6 R_E$ box runs also were carried out using two 4-year data sets. Comparing results from the various runs showed that almost all the unusual-looking localized variations such as those seen in the most distant x boxes in Figure 1 are not significant.

[17] Plasma density from the data-based models at each point along the field lines was used to evaluate integrals giving the number of particles in a unit flux tube

$$N(x_0, y_0) = \int (n/B) ds \quad (5)$$

(Figure 2). The density measured at the z at which the T89 integral started was used to evaluate that small portion of N which was determined using the T89 model. Most of the dawn-dusk asymmetry that is apparent in the most distant x boxes is not significantly larger than the statistical errors. Orbital effects on data sampling contributed to these statistical uncertainties. The asymmetry in Figure 2 was present in one 4-year data set but not in the other.

[18] Figure 2 shows that the average particle content of a unit flux tube drops substantially and fairly uniformly as one moves earthward. This general trend has been noted previously [Borovsky *et al.*, 1998; Garner *et al.*, 2003]. The average content of a unit flux tube crossing the neutral sheet at $x_0 = -29.5 R_E$ was 5.8×10^{21} ions plus an equal number of electrons per hemisphere. For flux tubes starting at $x_0 = -11.5 R_E$ the average was 1.8×10^{21} ions and electrons. An average flux tube at $x_0 = -11.5 R_E$ therefore contains only 30% as many particles as an average flux tube at $x_0 = -29.5 R_E$. Possible causes of this situation are discussed in section 5.

2.2. Deviations From Adiabatic Convection

[19] Equations (1) and (4) with $\gamma = 5/3$ describe the adiabatic properties of a plasma which is convecting and expanding or being compressed in the plasma sheet. These expressions are based on following a fixed group of particles which are confined within a real or imaginary

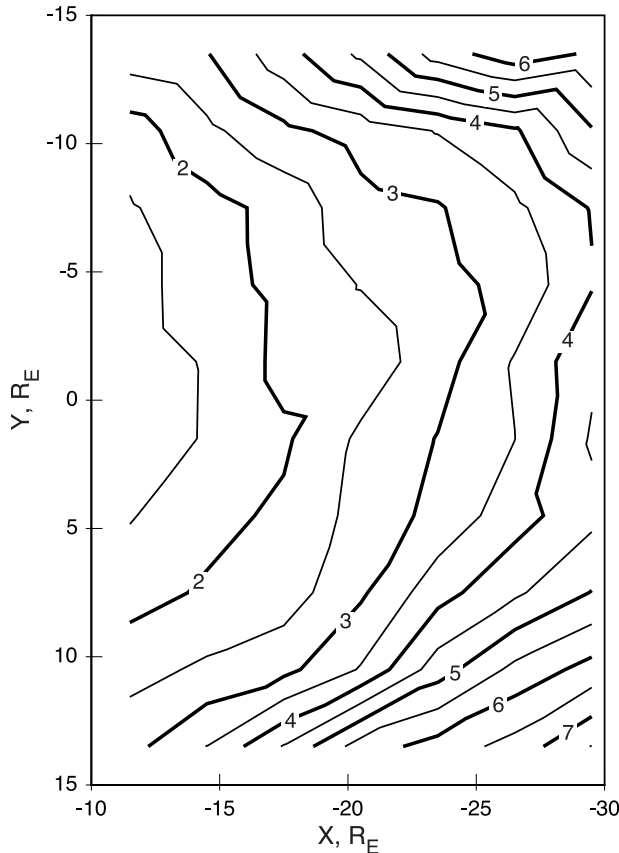


Figure 2. Number, N in 10^{21} particles, of ions and electrons per hemisphere within a unit flux tube.

box. The standard adiabatic equations do not apply to boxes with changing plasma content. The observed large depletion of particles in the more earthward flux tubes therefore requires further examination of equations (1) and (4).

[20] Figures 3 and 4 show how S_{σ}^V varies for ions and electrons. Figure 3 used $3 \times 3 R_E$ bins, and $6 \times 6 R_E$ bins were used for Figure 4. In these and other figures which compare ion and electron behavior, contour lines have been spaced at approximately equal fractional intervals to facilitate comparisons. The 3-D distributions of ion and electron pressures are similar to those presented previously [Kaufmann *et al.*, 2001], and the V from Figure 1 was used. In light of the decrease in flux tube content (Figure 2), it is not surprising that S_{σ}^V also decreases as one moves earthward. The averages of N , S_i^V , and S_e^V at $x_0 = -29.5 R_E$ are 3.2, 3.9, and 3.6 times their values at $x_0 = -11.5 R_E$, respectively.

[21] Our models and several other satellites have found that ions flow most nearly earthward at a location slightly dawnward of midnight [Angelopoulos *et al.*, 1993; Paterson *et al.*, 1998; Hori *et al.*, 2000]. Cross-tail flow was strongly duskward on the duskside of this y location and more weakly dawnward on the dawnside. The flow pattern we obtained using only the limited $|z| < 0.2 R_E$ data was erratic, became smoother when all the $|z| < 0.7 R_E$ data was averaged, and smoother still with all $|z| < 1.5 R_E$ data. The resulting average earthward flow and the dawnward flow on the dawnside decreased by 25% as the averaging region was extended from $|z| < 0.2$ to $|z| < 1.5 R_E$. The duskward flow on the duskside showed little z dependence

over this same region. The magnitudes of both components of the flow decreased when data from $|z| > 1.5 R_E$ was included in the averages. It has not been possible to directly measure electron convection paths with sufficient accuracy to carry out a similar analysis of electron flow.

[22] The solid and dashed curves in Figure 5 compare the x dependence of N and S_{σ}^V . The $-6 < y_0 < 3 R_E$ boxes from the $3 \times 3 R_E$ runs were averaged producing $3 \times 9 R_E$ x - y averages. This smoothed the plots but maintained $3 R_E$ resolution in the x direction. Figure 5 shows that the average number of particles in a unit flux tube decreased by 70% between $x_0 = -29.5$ and $-11.5 R_E$, while S_i^V and S_e^V decreased by 85% and 80%, respectively. These trends are continuing at the outer and inner limits of the region in which data are available, suggesting that studies covering a greater range of x_0 would see substantially larger percentage changes of N and S_{σ}^V . Examination of the box-to-box fluctuations gave statistical uncertainties of about 2% for each variable: N , S_i^V , and S_e^V . The more extensive smoothing associated with use of $6 \times 6 R_E$ boxes cut the differences between the drops in N and in S_{σ}^V almost in half. In each case, S_e^V dropped more rapidly than N and S_i^V dropped still more rapidly. These observations will be discussed in section 6.

3. Observed Temperature-Volume Relationships

[23] If particles are scattered, then the usual adiabatic invariants [Northrop, 1963] are not conserved. However, Wolf [1983] and Heinemann and Wolf [2001] showed that

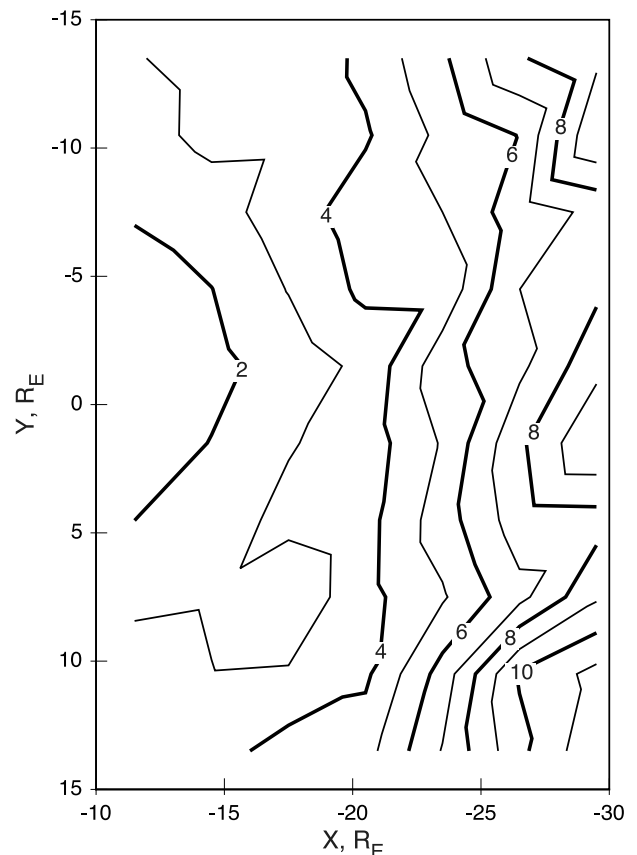


Figure 3. Spatial variations of S_i^V in 10^{16} Pa m^5 , defined in equation (1).

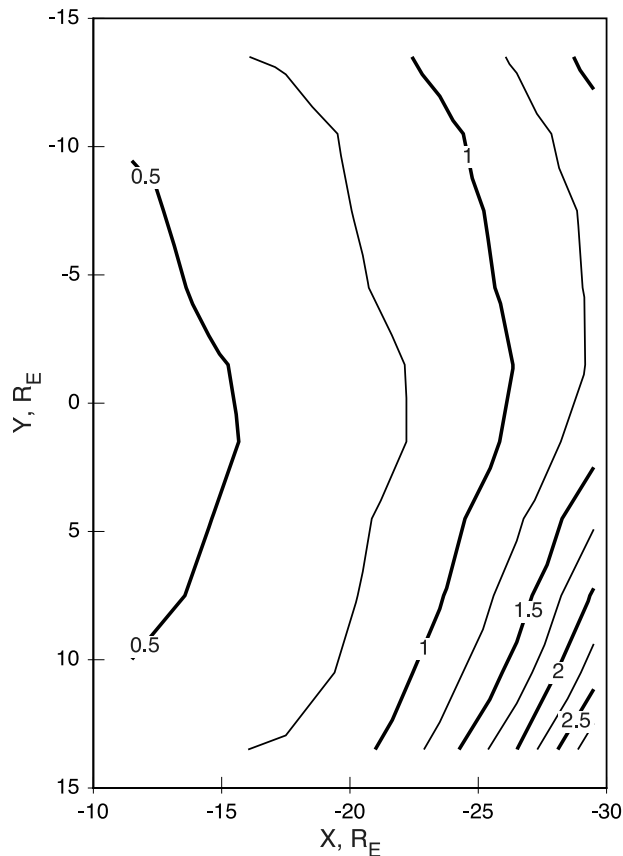


Figure 4. Similar to Figure 3, but for electrons and smoothed by using $6 \times 6 R_E$ boxes.

if a drifting group of particles is elastically scattered so that it remains isotropic, then an energy invariant (equation (3)) is conserved. Since λ_σ does not depend on the total number of particles in a unit flux tube, it would not be altered if an energy-independent loss process took place. Figures 6 and 7 are contour plots, based on $6 \times 6 R_E$ boxes, of λ_i and λ_e , respectively. The same $3 \times 9 R_E$ averages at $-6 < y_0 < 3 R_E$ that were used in Figure 5 showed that the ion invariant (Figure 6) decreased by 40% between $x_0 = -29.5$ and $-11.5 R_E$. The electron invariant (Figure 7) decreased by 11% over this same region. These figures suggest a nonadiabatic heat loss or the preferential depletion of the most energetic ions and, to a lesser extent, of the most energetic electrons in flux tubes nearest to the Earth. These observations will be combined with the S_σ^V and S_σ^n results in section 6.

4. Observed Pressure-Density Relationships

[24] The relationships described above required the use of long-term averages or empirical models to determine the volume of a unit flux tube. In contrast, P_σ and n_σ are available for every data point. For this reason a number of satellite data sets have been used to find a value of γ in equation (4) that makes S_σ^n most nearly uniform in the plasma sheet. Huang *et al.* [1989], Baumjohann and Paschmann [1989], Zhu [1990], Goertz and Baumjohann [1991], and Borovsky *et al.* [1998] studied different regions of the plasma sheet, used different data analysis methods, and obtained a variety of γ values.

[25] The spatial variations of S_σ^V and S_σ^n can be different if the average flux tube content decreases as one moves earthward. Consider the case of reconnection as an example. Assume a flux tube with an original equatorial crossing point of $x_0 = -30 R_E$ is suddenly separated into two objects by reconnection at $x = -20 R_E$. One object is a detached plasmoid containing half the volume and half the particles. The other object is a flux tube which is still attached to the Earth, containing the other half of the volume and particles. Immediately after this reconnection event, the attached portion of the flux tube would have the same P_σ and n_σ as it did before reconnection, but V and N would be reduced by half and the equatorial crossing point would have moved earthward by $10 R_E$. The value of S_σ^n would remain unchanged, so it would be the same as that of an $x_0 = -30 R_E$ flux tube. The value of S_σ^V would be $0.5^{5/3} = 0.32$ as large as the S_σ^V of an $x_0 = -30 R_E$ flux tube. Therefore if both S_σ^V and S_σ^n happened to be uniform throughout the plasma sheet before the reconnection event, S_σ^n would still be uniform but S_σ^V would decrease as one moved earthward. In the more general case of an initially nonuniform plasma sheet, N , S_σ^n , and S_σ^V all would be different from the values found in adjacent flux tubes which adiabatically convected from $x_0 = -30$ to $-20 R_E$ instead of having undergone reconnection. Since other particle depletion mechanisms can have different effects, an examination of both S_σ^V and S_σ^n appears to be worthwhile.

[26] Figure 8 shows contours of S_σ^n at $|z| < 0.2 R_E$ produced using $\gamma = 1, 5/3$, and $7/3$ from the $6 \times 6 R_E$ box runs. Similar plots were prepared at increments of $1/3$ from $\gamma = 1/3$ to $10/3$ for both ions and electrons. Since P_σ and n_σ were measured throughout the CPS, plots also were made using data taken at several z locations. This method of examining effects of different γ values is substantially different from previous techniques, which usually used plots of P_σ versus n_σ for individual data points.

[27] All plots using very small γ showed S_σ^n increasing rapidly as one moves earthward. Plots using very large γ showed S_σ^n decreasing earthward. Multiple peaks and valleys appeared when using the larger values of γ because this makes S_σ^n depend more sensitively on box-to-box fluctuations of n_σ . The electron plots were qualitatively similar to but more jagged than the ion plots. Changing the value of γ by only $1/3$ often produced plots that differed from each other by less than the box-to-box fluctuations. Our method therefore did not prove to be a very sensitive way to select a value of γ that makes S_σ^n most uniform. A plot similar to Figure 8 based on $\gamma = 5/3$ using data from only the first 4 years showed a dawnside peak in the $x = -16 R_E$ box but no peak on the duskside. A similar plot using only data from the second 4 years had two peaks on the duskside and none at dawn. The observations therefore did not detect any consistent non-uniformities of S_σ^n using $\gamma = 5/3$. The observations also did not reveal a value of γ that produced plots which were consistently more uniform throughout the plasma sheet than were plots based on $\gamma = 5/3$.

5. Analysis of Flux Tube Content

[28] Figures 2 and 5 showed that an average tube containing 1 Wb of magnetic flux which crosses the equator near $x_0 = -10 R_E$ contains only about 30% as many

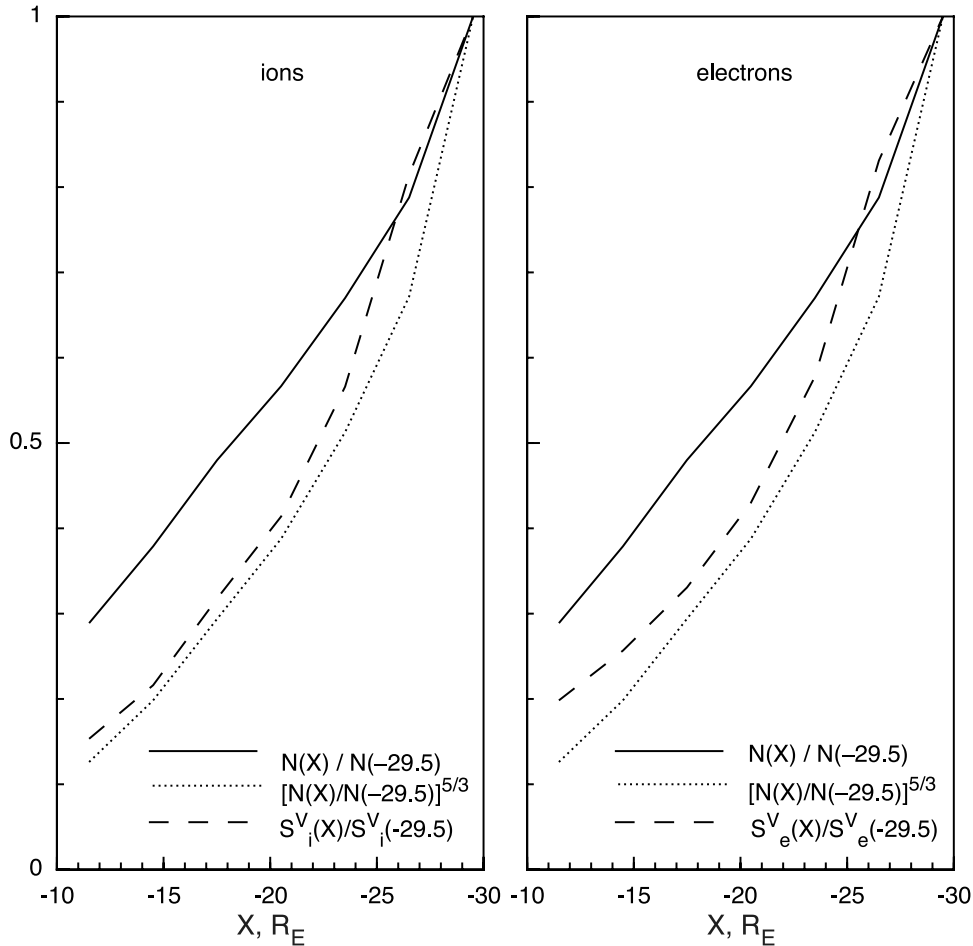


Figure 5. Comparison of the spatial variations of S_i^V and N using $3 \times 9 R_E$ boxes.

particles as does an average unit flux tube that is located near $x_0 = -30 R_E$. Mechanisms which have been proposed to explain this feature can be divided into two categories. In one set of mechanisms the individual flux tubes lose particles as they convect earthward. We include the loss of particles during reconnection in this category. The other mechanisms involve flux tubes with low N that drift earthward relative to flux tubes with high N .

5.1. Loss Through Flux Tube Ends

[29] Erickson [1992], Borovsky *et al.* [1998], and Garner *et al.* [2003] estimated how many ions are lost through the ends of flux tubes as they convect toward the Earth. These studies concluded that such losses are far smaller than the observed 70% depletion of flux tube content. The loss of energetic electrons and their replacement by low-energy ionospheric electrons to maintain charge neutrality is more rapid, but this does not alter the content of a unit flux tube. Precipitation into the ionosphere therefore does not appear to explain a major portion of the observed depletion of flux tube content.

5.2. Loss Through the Sides of a Flux Tube

[30] Ions with different energies have different guiding center gradient and curvature drift speeds, and these guiding center drifts are in the opposite direction for electrons. In

this section we include the drift associated with nonadiabatic effects such as the displacement seen on Speiser [1965] orbits in the gradient and curvature drift category and refer to $\mathbf{E} \times \mathbf{B}$ drift, which is the same for all particles, as the flux tube convection velocity.

[31] The effects of cross-tail drift were studied by Tsyganenko [1982], Kivelson and Spence [1988], and Garner *et al.* [2003], who concluded that the resulting particle loss is significant but not sufficient to explain the observed changes in N . These studies were based on the assumption that Liouville's theorem is valid in the plasma sheet or that the distribution function $f_\sigma(\mathbf{r}, \mathbf{v})$ remains constant when following a particle as it moves along a drift path in (\mathbf{r}, \mathbf{v}) space. Ions in these models generally drifted earthward, primarily as a consequence of $\mathbf{E} \times \mathbf{B}$ drift, and duskward, primarily as a consequence of gradient and curvature drifts. Garner *et al.* [2003] assumed that distribution functions are isotropic at the equator and that λ remains constant for a drifting particle so that $f_\sigma(\lambda, \mathbf{r})$ is conserved along a drift path. As a result, particles with different energies or different λ that reach a point such as $x = -20 R_E, y = 0$ could be traced back to different y locations at a more distant x . The problem encountered was that $f_\sigma(\lambda, \mathbf{r})$ was smaller at $x = -10$ to $-20 R_E$ than at $x = -30$ to $-50 R_E$ for almost all λ . For example, $f_i(\lambda = 6500, x = -10, y = 0)$ was larger than $f_i(\lambda = 6500, x = -30, y)$ at all y except

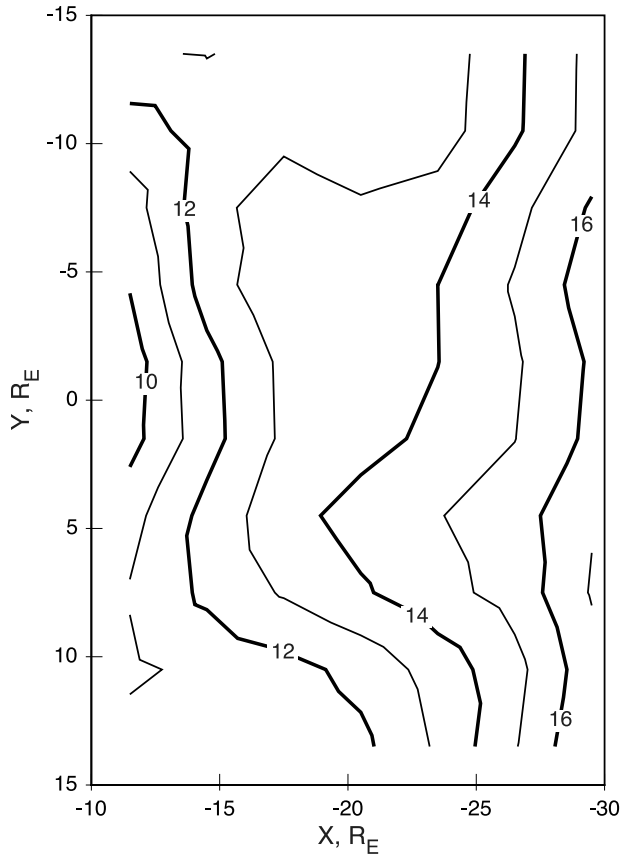


Figure 6. Spatial variations of the ion energy parameter $T_i v^{2/3}$ in 10^7 eV m^2 .

at the low-latitude boundary layer (LLBL), where there are few energetic ions. In the above expressions, the units of x and y are R_E and λ is in $eV \cdot (R_E/nT)^{-2/3}$. The invariant $\lambda = 6500$ corresponds to energies of 3.9 keV at $x = -10 R_E$ and 1.9 keV at $x = -30 R_E$. Since this radial variation was found for almost all λ , it was concluded that particles which adiabatically drift from $x = -30 R_E$ to $x = -10 R_E$ near midnight would have a larger $f_i(\lambda, \mathbf{r})$ than is observed. It is only the small number of high-energy ions that can drift to midnight from the LLBL that would bring in particles with small $f_i(\lambda, \mathbf{r})$ and therefore contribute to a reduction in N . Garner *et al.* [2003] therefore concluded that adiabatic drift alone could not explain the magnitude of the observed reduction of N .

[32] The $-6 < y_0 < 3 R_E$ boxes were selected for our study to illustrate this problem (Figure 5) because it is here that the total ion drift velocity is most nearly earthward. Figure 2 shows that there is relatively little cross-tail gradient of N within $5 R_E$ of midnight. A uniform cross-tail drift through the sides of flux tubes therefore would contribute little to changes of N in this region. Plots similar to Figure 5 but for other y_0 locations show that the x dependence of these parameters are similar out to $|y_0| = 9 R_E$. Uniform gradient and curvature cross-tail drifts through the sides of flux tubes therefore would not provide a dominant flux tube depletion mechanism near midnight.

[33] We have not used measured bulk velocities to determine the loss by nonuniform or nonadiabatic drift through the sides of flux tubes for several reasons. One is

that the measured flow velocities represent local drifts rather than averaged drifts. Previous 2-D data-based studies [Angelopoulos *et al.*, 1992; Ashour-Abdalla *et al.*, 1998; Hori *et al.*, 2000; Kaufmann *et al.*, 2001] suggested that the total cross-tail ion flow in the CPS involves a combination of two effects. There are duskward gradient, curvature, and diffusive drifts of ions and there also is a tendency for $\mathbf{E} \times \mathbf{B}$ drift to have a component away from midnight. Dawnward and duskward convective drifts of flux tubes away from midnight would be associated with an earthward component of \mathbf{E} on the dawnside and a tailward component of \mathbf{E} on the duskside. Such convection involves a large divergence of flow in the x - y plane. Drift in the z direction toward the neutral sheet is needed to maintain continuity in a long-term-averaged model. It is this flow in the z direction that is hard to measure accurately on a satellite such as Geotail, whose spin axis is near the GSE z axis.

5.3. Reconnection

[34] It was noted previously that reconnection produces a sudden reduction in the content of a unit flux tube and a simultaneous earthward jump of the equatorial end of the portion of the flux tube that is attached to the ionosphere. A problem with attributing all the variation of N (Figures 2 and 5) to particle ejection in plasmoids is that reconnection typically takes place beyond $x_0 = -20 R_E$ [Nagai *et al.*, 1998] while the rapid decrease of N continues well earthward of this point. In fact, Borovsky *et al.* [1998] concluded that most depletion takes place between $x_0 = -15$ and $-6.6 R_E$.

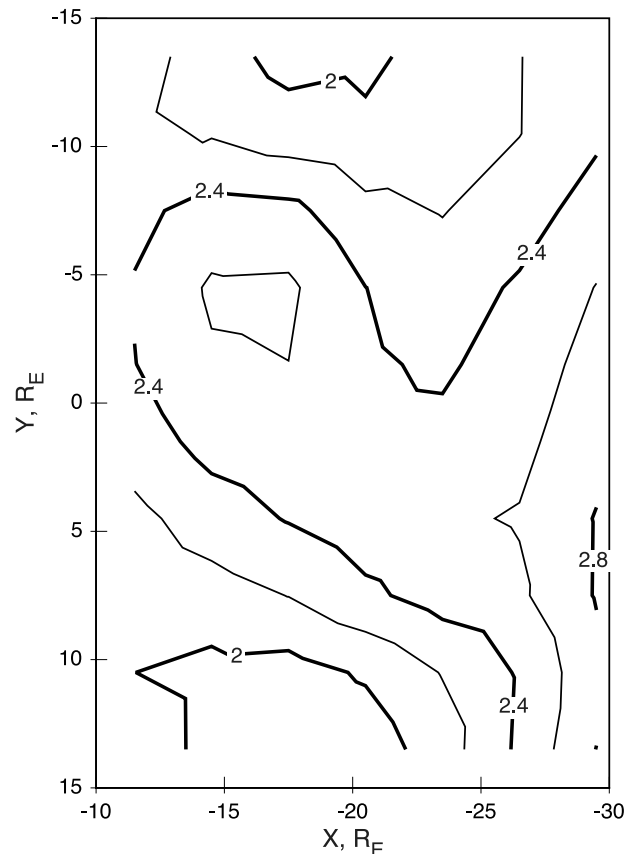


Figure 7. Similar to Figure 6, but for electrons.

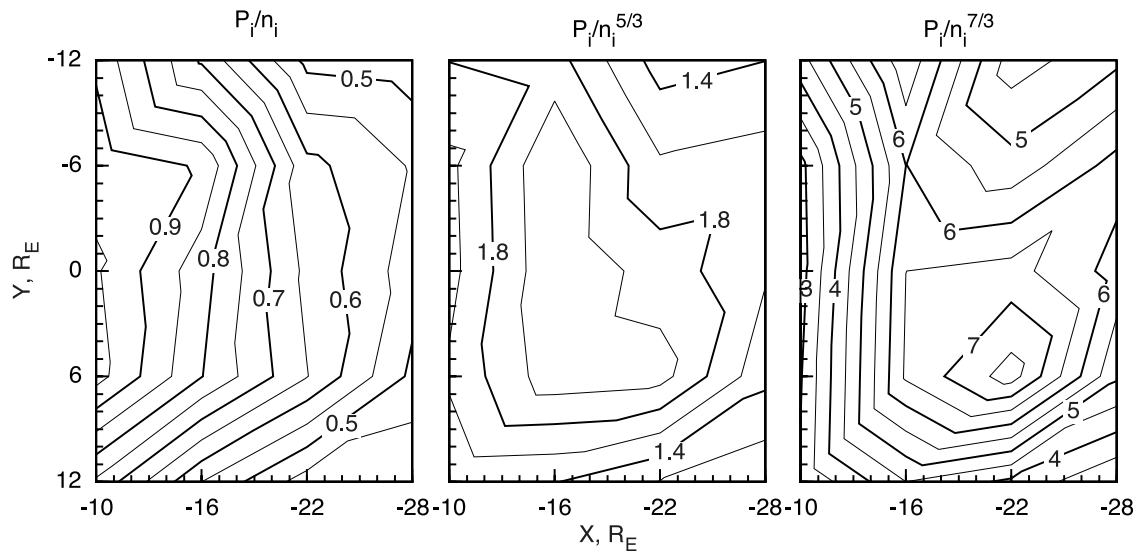


Figure 8. Spatial variations of S_i^η , defined in equation (4), for three values of γ .

[35] To illustrate why it is hard to attribute depletion near the Earth to reconnection, Figure 9 shows the percentage of points with $B_z < 0$ that were seen at $|z| < 0.2 R_E$. Negative B_z is an indication that reconnection has taken place earthward of the satellite. On average, B_z is negative 7% of the time in the most distant $6 \times 6 R_E$ boxes, centered at $x_0 = -28 R_E$, but only 0.4% of the time in the most earthward boxes, centered at $x_0 = -10 R_E$. The absence of negative B_z points is most dramatic in the $x_0 = -10, |y_0| < 9 R_E$ boxes. Only five of the 3700 points in these boxes at $|z| < 0.2 R_E$ and only nine of the 7600 points at $|z| < 0.7 R_E$ had $B_z < 0$.

[36] We conclude that the direct effects of reconnection can contribute significantly to the earthward decline of N between $x_0 = -30$ and $-20 R_E$. The scarcity of evidence for reconnection below $x_0 = -15 R_E$ makes it difficult to explain the continued rapid decline of N at lower altitudes as the direct effect of particle loss in detached plasmoids. Since we have used 1-min averages, some brief reconnection events undoubtedly were missed. As will be discussed below, reconnection at $x < -20 R_E$ also can indirectly cause a reduction of N at low altitudes through the interchange processes. Reconnection could produce the high-altitude flux tubes with reduced N which preferentially drift earthward.

5.4. Bubbles and Blobs

[37] *Pontius and Wolf* [1990] suggested that the observed reduction of S_σ^V in the inner plasma sheet could be produced by the differential drift of flux tubes if a magnetotail plasma source created bubbles and blobs. The bubbles or flux tubes with small n_σ , N , and S_σ^V would polarize and drift earthward relative to adjacent blobs or flux tubes which happen to have larger n_σ , N , and S_σ^V . It was proposed that the bubbles dissipate by diffusion in the inner plasma sheet. This interchange would result in N and S_σ^V gradients in the sense shown in Figures 2 through 5.

[38] Studies by *Angelopoulos et al.* [1992] and *Schödel et al.* [2001] were directed at examining the importance of bursty bulk flow (BBF) events in the plasma sheet. Superposed epoch analyses were used to determine the average variations of plasma parameters near the time of peak bulk flow. These studies found relatively small density and

pressure fluctuations and larger temperature and magnetic field changes during the flow bursts. *Chen and Wolf* [1993, 1999] suggested that the BBF events could be the proposed bubbles and blobs even though the density fluctuations are small relative to the observed 70% reduction of N . They pointed out that flux tube content can be different on adjacent flux tubes even when the densities and pressures are equal at the neutral sheet if the flux tubes have significantly different shapes. The shapes of BBF flux tubes are likely to be significantly different from the shapes of

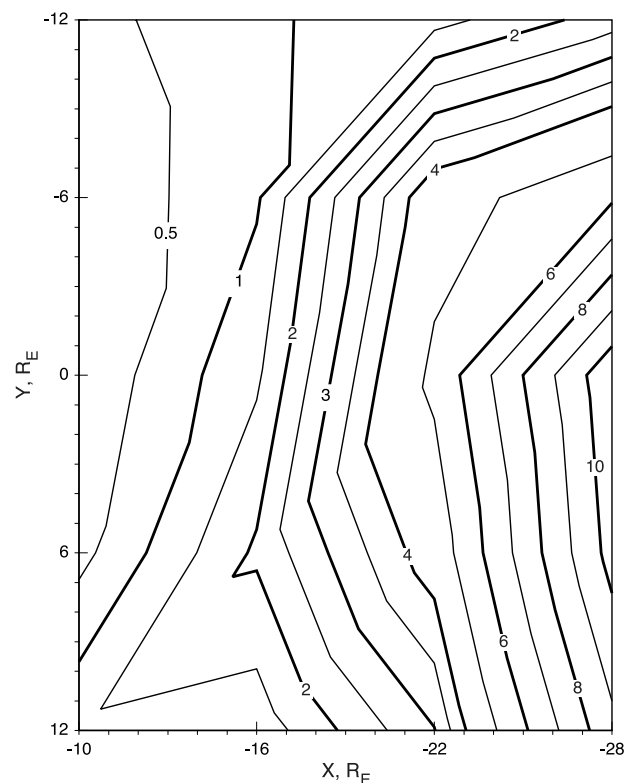


Figure 9. Percentage of data points with negative B_z .

other magnetotail flux tubes. This topic is discussed in section 6.

5.5. Phase Space Holes and Clumps

[39] The hole and clump instability is a mechanism that generates very small structures containing reduced and enhanced densities throughout an unstable region such as a bursty bulk flow channel. Holes are small structures in which the number of particles is depleted within a limited velocity region. This depletion of particles with certain velocities also decreases the total number density of particles at the location of the hole. The kinetic version of the clump and hole instability was introduced by Dupree [1982]. This mechanism has been studied using simulations [Berman *et al.*, 1985] and it has been applied to the acceleration of auroral electrons [Tetreault, 1991]. In this latter application the perpendicular structure of clumps or holes generates electrostatic ion cyclotron waves and the parallel structure produces double layers. Holes are self-binding structures which form equilibrium Bernstein-Greene-Kruskal (BGK) modes when isolated from other structures. When followed in time, they appear as phase space eddies of the BGK modes.

[40] Kinetic ion holes in the plasma sheet would have small scale sizes, on the order of 10 Debye lengths or a few kilometers. Such objects would pass over a satellite in tenths or hundredths of a second. Electric field or possibly Langmuir probe detectors are more likely than particle detectors to observe such objects. The clump and hole instabilities can be driven either by field aligned or by cross-field currents.

[41] An MHD version of the clump instability also has been discussed by Tetreault [1989]. This extended BGK mode is similar to the tearing mode instability which was studied by Schindler [1975], Galeev [1982], and others. The possible significance of hole and tearing mode instabilities is that they can continually produce regions of reduced plasma density and other regions of enhanced plasma density throughout a channel in which currents are sufficiently strong to drive these instabilities. The continuous formation of many weak density depletions along an average drift path could explain the observed 70% depletion of the average flux tube content if the instability region is large even when each hole drifts only a small distance earthward before it merges into the adjacent plasma.

6. Analysis of Pressure, Volume, Density Relationships

[42] Adiabatic properties of the plasma sheet are studied by following the flow of individual flux tubes. Since we have only long-term averages of the fluid parameters, it is necessary to regard the plasma sheet as a time-independent flow field containing steady-state fluctuations. This steady-state assumption is used here to examine the observed spatial variations of fluid parameters such as S_σ^V , S_σ^a , λ_σ , and N .

6.1. Comparison of S_σ^V and λ_σ

[43] Combining the definitions of S_σ^V and λ_σ in equations (1) and (3) with $P_\sigma = nT_\sigma$ and $N = nV$ gives

$$S_\sigma^V = N\lambda_\sigma. \quad (6)$$

The above expression for N is based on the assumption that the electron and ion number densities are equal and constant along an average flux tube. The actual evaluation of N shown in Figure 2 used the measured ion n_i , which fluctuated along an average field line. The measured density tended to increase as one moved earthward along an average magnetic field line near midnight and to decrease as one moved earthward near the flanks. Typical changes were 25%, which is comparable to the uncertainties in these boxes.

[44] Using the $-6 < y_0 < 3 R_E$ boxes where the total flow is generally in the x direction as an example (Figure 5), equation (6) relates the variations of S_σ^V , λ_σ , and N along this drift path by

$$\frac{dS_\sigma^V}{dx} = N \frac{d\lambda_\sigma}{dx} + \lambda_\sigma \frac{dN}{dx}. \quad (7)$$

Figures 6 and 7 show that λ_σ , which would be invariant if particles were elastically scattered as they convected, actually has some x dependence. If λ_σ was constant then equation (7), when normalized by dividing by $S_\sigma^V(-29.5) = \lambda_\sigma N(-29.5)$, shows that the dashed and solid curves in Figure 5 would be related by

$$\frac{d}{dx} \left[\frac{S_\sigma^V(x)}{S_\sigma^V(-29.5)} \right] = \frac{d}{dx} \left[\frac{N(x)}{N(-29.5)} \right]. \quad (8)$$

As might be expected, equation (8) predicts that these two curves in Figure 5 would be identical. The relatively small difference between the S_σ^V and N curves therefore may be associated with the changes in λ_σ and to inaccuracies associated with the assumption that n is constant along a field line. Data from Figures 2, 6, and 7 show that the $Nd\lambda_\sigma/dx$ term, which was neglected in deriving equation (8), is almost half and approximately 10% as large as the $\lambda_\sigma dN/dx$ term near midnight for ions and electrons, respectively. These figures varied substantially for different y_0 locations and when $6 \times 6 R_E$ binning was used, but the term involving $d\lambda_\sigma/dx$ was consistently larger for ions than for electrons and smaller than the term involving dN/dx .

[45] The spatial dependencies of S_σ^V and λ_σ described above suggest that energy is lost from flux tubes that move with the average drift velocity. Since gradient and curvature drifts are energy-dependent, cross-tail drift could be important in reducing the density of the highest energy ions and electrons. This mechanism would produce the observed larger effect on T_i than on T_e because the ions are more energetic and therefore drift faster than the electrons. Figures 6 through 10 of Garner *et al.* [2003] show the specific high-energy ions whose drift paths in their model trace back from an observer at midnight to a source at the LLBL. Since plasma at the LLBL does not contain many high-energy ions, one would expect to see a lack of such particles in the distribution functions measured at midnight and therefore reduced N and S_σ^V .

[46] Other mechanisms also could explain the observed variations of S_σ^V and λ_σ . Auroral processes and ionospheric Joule heating require a large source of energy which flows down to the ionosphere. Borovsky *et al.* [1998] showed that if most of this energy were removed from plasma sheet ions, then a large fraction of the energy in a convecting flux tube

would be depleted. Such processes could involve instabilities which excite Alfvén or other wave modes. Drifts which generate electric fields through charge separation also can remove energy from plasma sheet ions. In the future it may be possible to evaluate heat fluxes using the data-based models. An analysis of heat fluxes and other terms in the energy equation has not yet been attempted because errors can become large when determining these high-order terms.

6.2. Comparison of S_σ^V and S_σ^n With $\gamma = 5/3$

[47] It was found above that the use of $\gamma = 5/3$ made the spatial distribution of S_σ^n as uniform as any other choice of γ . We will therefore assume $\gamma = 5/3$ in this section. The variables S_σ^V and S_σ^n would be equal if the flux tube content N had no spatial variation and if the particle density n_σ was constant along field lines. However Figures 2 and 5 show that there are large variations in N along average drift paths. Equations (1), (4) with $\gamma = 5/3$, and the equations above (6) can be combined to examine the difference between S_σ^V and S_σ^n

$$\frac{S_\sigma^V}{S_\sigma^n} = N^{5/3}, \quad (9)$$

again assuming that n_i and n_e are equal and constant along an average field line. Equation (9) shows that if S_σ^V and $N^{5/3}$ had the same spatial dependence along a drift path, then S_σ^n would be constant along that drift path. Comparing the dotted and dashed lines in Figure 5 shows that the x dependencies of $N^{5/3}$ and S_σ^V are similar. This is another way to view the fact that S_σ^n with $\gamma = 5/3$ is relatively uniform, as shown in Figure 8.

[48] We can try to examine some aspects of the bubbles and blobs mechanism using the superposed epoch BBF results described previously [Angelopoulos *et al.*, 1992; Schödel *et al.*, 2001] plus the discussion of differences between N , S_σ^V , and S_σ^n . Only small fluctuations of n_i were seen in the superposed epoch studies during the intervals of rapid earthward flow. There were no substantial differences between n_i well before and well after the events. There was a net increase of P_i when comparing times well after to well before the events, but only small changes of P_i were seen at the times of fastest flow. Sergeev *et al.* [1996] found some fast flow events with substantially reduced plasma pressures, but the superposed epoch studies noted above did not find large density or pressure depletions in average events. The minor changes of n_i and P_i during the peak flow intervals shows that S_σ^n was at most only slightly larger when flows were most rapid, but S_σ^V was significantly larger well after than well before an event.

[49] The principal question to be addressed is whether N and S_σ^V are reduced during flow bursts. One observation is that the average B_z increased by 10% or more during the minute containing the fastest flows and stabilized by 10 min after the events at a level about 30% above the level seen 10 min before the events. Since B_z is fairly uniform throughout the central plasma sheet, this suggests that B_z at the neutral sheet increased similarly. As a result, the cross-sectional area of a unit flux tube, $1/B$, decreased by about 10% and the shapes of field lines changed during the brief fast flow periods. Larger changes in the same sense developed after the time of peak flow velocity. However,

since the increase of B_z both reduces the cross-sectional area and increases the length of a flux tube with a given (x_0, y_0) it is difficult to predict how $V(x_0, y_0)$, $N(x_0, y_0)$, and $S_\sigma^V(x_0, y_0)$ will change. Figure 5 shows that a process that reduces S_σ^V near midnight by 15% is needed for every 2.5 R_E segment along the drift path. We conclude that the previously reported BBF observations are not sufficient to determine whether interchange can explain the observed 70% average reductions of N and 80–85% average reduction of S_σ^V . We hope to be able to resolve this question in a future study using sets of 3-D models.

[50] A related mechanism that may make it easier to explain the structure seen in Figures 2 through 5 involves assuming that the entire BBF flow channels are regions of low N and S_σ^V . If this correlation is found to exist, then both the faster and the slower drifting flux tubes within the BBF flow channels could be characterized by N and S_σ^V , which are small relative to the values in flux tubes outside the channels. The BBF channels then would bring low N and low S_σ^V flux tubes earthward as long as these channels existed. This mechanism could also require some heat flow to explain the magnitude of the S_σ^V changes.

[51] It would be necessary to generate sets of 3-D models of average flux tubes during fast and slow flow events to quantitatively determine whether the above suggestions are sufficient to explain the observed variations of N and S_σ^V . The volumes and shapes of fast and slow flow flux tubes then could be compared. This project would require a substantial amount of fast flow data in each (x, y, β_x) box. It also would be necessary to identify flux tubes with a given equatorial crossing point in measurements made at all z . We plan to explore the possibility of making fast flow models so that field lines and the average V , N , and S_σ^V can be determined for these special time periods.

7. Summary

[52] Several thermodynamic parameters were examined using long-term-averaged data-based models of the plasma sheet. The characteristics of the models that make them particularly suitable for the present study are that they are three-dimensional, force balanced, and involve a consistent combination of plasma and magnetic field data sets. The models used in the present study were averages over data for all geomagnetic and solar wind conditions.

[53] The principal contribution of this paper was the creation of plots that show details of the variations of a set of plasma parameters throughout the $-30 < x < -10 R_E$, $|y| < 15 R_E$ region. Our 3-D models were used to integrate along average field lines and therefore to evaluate $V(x_0, y_0)$, the volume of a unit flux tube and $N(x_0, y_0)$, the particle content of a unit flux tube that crosses the equator at (x_0, y_0) . Plots of $N(x_0, y_0)$ showed in more detail the spatial variations which had been found in previous studies. An average unit flux tube at $x = -10 R_E$ contained only 30% as many particles as an average unit flux tube at $x = -30 R_E$. This information was then used to examine the spatial variations of the parameters $S_\sigma^V = P_\sigma V^{5/3}$, $\lambda_\sigma = T_\sigma V^{2/3}$, and $S_\sigma^n = P_\sigma/n_\sigma^\gamma$, all of which would be constant along drift paths under certain conditions.

[54] The paper included a brief survey of mechanisms that have been proposed to explain the nonadiabatic features

of the plasma sheet. Some spatial variation of $N(x_0, y_0)$ could be produced by loss out the ends and by drift through the sides of flux tubes. Previous studies [e.g., *Garner et al.*, 2003] showed that loss out the ends is not important and that drift effects are important but not sufficient to explain the large earthward decrease of $N(x_0, y_0)$. We did not carry out a separate study using flow velocities from the 3-D data-based models. Ion bulk flow velocities, particularly those in the z direction, are difficult to measure with sufficient accuracy. Reconnection is likely to contribute to the depletion of particles beyond $x = -20 R_E$ but does not appear to be adequate at lower altitudes. Instabilities such as the interchange of bubbles and blobs [*Pontius and Wolf*, 1990], phase space clumps and holes, or properties of fast flow channels could be important and were considered briefly. We hope to examine these topics in more detail in the future.

[55] A comparison of S_σ^V and λ_σ was carried out. Most of the variations of these two parameters could be attributed to variations of N . The differences between variations of S_σ^V and λ_σ suggested that the most energetic particles were being preferentially depleted or decelerated as flux tubes moved earthward. Depletion could be caused by drift effects, which are energy-dependent, or by the flow of heat flux to the ionosphere.

[56] It was found that the selection of $\gamma = 5/3$ was as good as any choice for explaining the structure of S_σ^n . A comparison of spatial variations of S_σ^V with those of S_σ^n showed that the mechanisms listed above also could provide important contributions to these observations. However, more detailed studies using a series of models sorted according to geophysical or solar wind parameters will be needed before definitive separations between the proposed mechanisms can be made.

[57] **Acknowledgments.** This material is based upon work supported by the National Science Foundation under grants ATM-9730845 and ATM-0122618 and by the National Aeronautics and Space Administration under grant NAG5-11820 at the University of New Hampshire. Research at the University of Iowa was supported by the National Aeronautics and Space Administration under grant NAG5-11485. The authors would like to thank S. Kokubun who supplied full Geotail magnetic field measurements throughout the period studied.

[58] Lou-Chuang Lee thanks the two reviewers for their assistance in evaluating this paper.

References

- Angelopoulos, V., W. Baumjohann, C. F. Kennel, F. V. Coroniti, M. G. Kivelson, R. Pellat, R. J. Walker, H. Lühr, and G. Paschmann (1992), Bursty bulk flows in the inner central plasma sheet, *J. Geophys. Res.*, *97*, 4027–4039.
- Angelopoulos, V., et al. (1993), Characteristics of ion flow in the quiet state of the inner plasma sheet, *Geophys. Res. Lett.*, *20*, 1711–1714.
- Ashour-Abdalla, M., et al. (1998), Determination of particle sources for a Geotail distribution function observed on May 23, 1995, in *Geospace Mass and Energy Flow*, edited by J. L. Horwitz et al., pp. 297–312, AGU, Washington, D.C.
- Baumjohann, W., and G. Paschmann (1989), Determination of the polytropic index in the plasma sheet, *Geophys. Res. Lett.*, *16*, 295–298.
- Berman, R. H., D. J. Tetreault, and T. H. Dupree (1985), Simulation of phase space hole growth and the development of intermittent plasma turbulence, *Phys. Fluids*, *28*, 155–176.
- Borovsky, J. E., R. C. Elphic, H. O. Funsten, and M. F. Thomsen (1997), The Earth's plasma sheet as a laboratory for flow turbulence in high- β MHD, *J. Plasma Phys.*, *57*, 1–34.
- Borovsky, J. E., M. F. Thomsen, and R. C. Elphic (1998), The driving of the plasma sheet by the solar wind, *J. Geophys. Res.*, *103*, 17,617–17,639.
- Chen, C. X., and R. A. Wolf (1993), Interpretation of high-speed flows in the plasma sheet, *J. Geophys. Res.*, *98*, 21,409–21,419.
- Chen, C. X., and R. A. Wolf (1999), Theory of thin-filament motion in Earth's magnetotail and its application to bursty bulk flows, *J. Geophys. Res.*, *104*, 14,613–14,626.
- Dupree, T. H. (1982), Theory of phase-space holes, *Phys. Fluids*, *25*, 277–289.
- Erickson, G. M. (1992), A quasi-static magnetospheric convection model in two dimensions, *J. Geophys. Res.*, *97*, 6505–6522.
- Erickson, G. M., and R. A. Wolf (1980), Is steady convection possible in the Earth's magnetotail?, *Geophys. Res. Lett.*, *7*, 897–900.
- Frank, L. A., K. L. Ackerson, W. R. Paterson, J. A. Lee, M. R. English, and G. L. Pickett (1994), The comprehensive plasma instrumentation (CPI) for the GEOTAIL spacecraft, *J. Geomag. Geoelectr.*, *46*, 23–37.
- Galeev, A. A. (1982), Magnetospheric tail dynamics, in *Magnetospheric Plasma Physics*, edited by A. Nishida, pp. 143–196, D. Reidel, Norwell, Mass.
- Garner, T. W., R. A. Wolf, R. W. Spiro, M. F. Thomsen, and H. Korth (2003), Pressure balance inconsistency exhibited in a statistical model of magnetospheric plasma, *J. Geophys. Res.*, *108*(A8), 1331, doi:10.1029/2003JA009877.
- Goertz, C. K., and W. Baumjohann (1991), On the thermodynamics of the plasma sheet, *J. Geophys. Res.*, *96*, 20,991–20,998.
- Hau, L.-N., R. A. Wolf, G.-H. Voigt, and C. C. Wu (1989), Steady state magnetic field configurations for the Earth's magnetotail, *J. Geophys. Res.*, *94*, 1303–1316.
- Heinemann, M., and R. A. Wolf (2001), Relationships of models of the inner magnetosphere to the Rice Convection Model, *J. Geophys. Res.*, *106*, 15,545–15,554.
- Hori, T., K. Maezawa, Y. Saito, and T. Mukai (2000), Average profile of ion flow and convection electric field in near-Earth plasma sheet, *Geophys. Res. Lett.*, *27*, 1623–1626.
- Huang, C. Y., C. K. Goertz, L. A. Frank, and G. Rostoker (1989), Observational determination of the adiabatic index in the quiet time plasma sheet, *Geophys. Res. Lett.*, *16*, 563–566.
- Israelevich, P. L., A. I. Ershkovich, and N. A. Tsyganenko (2001), Magnetic field and electric current density distribution in the geomagnetic tail based on Geotail data, *J. Geophys. Res.*, *106*, 25,919–25,927.
- Kaufmann, R. L., B. M. Ball, W. R. Paterson, and L. A. Frank (2001), Plasma sheet thickness and electric currents, *J. Geophys. Res.*, *106*, 6179–6193.
- Kaufmann, R. L., C. Lu, W. R. Paterson, and L. A. Frank (2002), Three-dimensional analyses of electric currents and pressure anisotropies in the plasma sheet, *J. Geophys. Res.*, *107*(A7), 1103, doi:10.1029/2001JA000288.
- Kaufmann, R. L., W. R. Paterson, and L. A. Frank (2003), Birkeland currents in the plasma sheet, *J. Geophys. Res.*, *108*(A7), 1299, doi:10.1029/2002JA009665.
- Kivelson, M. G., and H. E. Spence (1988), On the possibility of quasi-static convection in the quiet magnetotail, *Geophys. Res. Lett.*, *15*, 1541–1544.
- Kokubun, S., T. Yamamoto, M. H. Acuna, K. Hayashi, K. Shiokawa, and H. Kawano (1994), The Geotail magnetic field experiment, *J. Geomag. Geoelectr.*, *46*, 7–21.
- Lemon, C., F. Toffoletto, M. Hesse, and J. Birn (2003), Computing magnetospheric force equilibria, *J. Geophys. Res.*, *108*(A6), 1237, doi:10.1029/2002JA009702.
- Nagai, T., M. Fujimoto, Y. Saito, S. Machida, T. Terasawa, R. Nakamura, T. Yamamoto, T. Mukai, A. Nishida, and S. Kokubun (1998), Structure and dynamics of magnetic reconnection for substorm onsets with Geotail observations, *J. Geophys. Res.*, *103*, 4419–4440.
- Northrop, T. G. (1963), *The Adiabatic Motion of Charged Particles*, John Wiley, Hoboken, N. J.
- Paterson, W. R., L. A. Frank, S. Kokubun, and T. Yamamoto (1998), Geotail survey of ion flow in the plasma sheet: Observations between 10 and 50 R_E , *J. Geophys. Res.*, *103*, 11,811–11,825.
- Pontius, D. H., and R. A. Wolf (1990), Transient flux tubes in the terrestrial magnetosphere, *Geophys. Res. Lett.*, *17*, 49–52.
- Schindler, K. (1975), Plasma and fields in the magnetospheric tail, *Space Sci. Rev.*, *17*, 589–614.
- Schindler, K., and J. Birn (1982), Self-consistent theory of time-dependent convection in the Earth's magnetotail, *J. Geophys. Res.*, *87*, 2263–2275.
- Schödel, R., W. Baumjohann, R. Nakamura, V. A. Sergeev, and T. Mukai (2001), Rapid flux transport in the central plasma sheet, *J. Geophys. Res.*, *106*, 301–313.
- Sergeev, V. A., V. Angelopoulos, J. T. Gosling, C. A. Cattell, and C. T. Russell (1996), Detection of localized, plasma-depleted flux tubes or bubbles in the midtail plasma sheet, *J. Geophys. Res.*, *101*, 10,817–10,826.
- Speiser, T. W. (1965), Particle trajectories in model current sheets: 1. Analytic solutions, *J. Geophys. Res.*, *70*, 4219–4226.

- Tetreault, D. J. (1989), Steady-state magnetohydrodynamic clump turbulence, *Phys. Fluids B*, *1*, 511–523.
- Tetreault, D. (1991), Theory of electric fields in the auroral acceleration region, *J. Geophys. Res.*, *96*, 3549–3563.
- Tsyganenko, N. A. (1982), On the convective mechanism for formation of the plasma sheet in the magnetospheric tail, *Planet. Space Sci.*, *30*, 1007–1012.
- Tsyganenko, N. A. (1989), A magnetospheric magnetic field model with a warped tail current sheet, *Planet. Space Sci.*, *37*, 5–20.
- Wolf, R. A. (1983), The quasi-static (slow-flow) region of the magnetosphere, in *Solar-Terrestrial Physics*, edited by R. L. Carovillano and J. M. Forbes, pp. 303–368, D. Reidel, Norwell, Mass.
- Zaharia, S., and C. Z. Cheng (2003), Can an isotropic plasma pressure distribution be in force balance with the T89 model field?, *J. Geophys. Res.*, *108*(A11), 1412, doi:10.1029/2002JA009501.
- Zhu, X. M. (1990), Plasma sheet polytropic index as inferred from the FPE measurements, *Geophys. Res. Lett.*, *17*, 2321–2324.
-
- L. A. Frank and W. R. Paterson, Department of Physics and Astronomy, University of Iowa, Iowa City, IA 52242, USA. (frank@iowasp.physics.uiowa.edu; william-paterson@uiowa.edu)
- R. L. Kaufmann, Department of Physics, University of New Hampshire, Durham, NH 03824, USA. (dick.kaufmann@unh.edu)